JOURNAL OF MATERIALS SCIENCE 30 (1995) 3207–3215

Experimental characterization of permeability and fibre wetting for liquid moulding

D. A. STEENKAMER, S. H. MCKNIGHT, D. J. WILKINS, V. M. KARBHARI
Department of Applied Mechanics and Engineering Sciences, University of California, San Diego, La Jolla, CA 92093, USA

Liquid moulding processes are unique in that resin is infused into a dry fibre preform. Appropriate wet-out of the reinforcing fibres is thus a necessity for the achievement of good composite properties. For this class of manufacturing methods, both macroscopic flow, as related to Darcy's Law and characterized by permeability, and microscopic flow, as related to fibre wet-out, are important. The current research investigates factors affecting permeability and fibre wet-out as related to liquid moulding. Specifically, it is shown that fabric permeability is dependent on the type of test fluid used. Surface tension and contact angle measurements indicate that interactions at the microscopic level between fibre and test fluid account for these differences in permeability. The investigation illustrates the competing nature of macroscopic and microscopic flow in liquid moulding.

1. Introduction

Liquid moulding (LM) processes, most notably resin transfer moulding and structural reaction injection moulding, have become increasingly popular during the past fifteen years for the production of complex composite parts. Once used primarily by the commodities industry to make parts ranging from bath tubs [1] to computer terminal housings [2], these processes have evolved and are currently being investigated for use in the fabrication of structural parts for automobiles [3] and commercial and military aircraft [4]. This LM evolution has come about, in part, due to the composites industry's desire to lessen part cost while still meeting prescribed performance requirements.

In its most basic form, LM is a two-step process: fibre preforming followed by resin infusion and cure. In the first stage, reinforcing fibres are arranged and combined (possibly with cores and inserts) into a skeleton of the actual part in order to satisfy microstructural and geometric requirements. The preform is then loaded into the mould and the mould is closed. The second phase of the process involves the transfer of resin from holding tanks into the mould. During the infusion process, the resin flows through the preform, "wets-out" the individual fibre bundles, and polymerizes. Once the composite develops sufficient dimensional stability, it may be removed from the mould and post-cured (if needed) to complete the crosslinking reaction. A schematic of this process is shown in Fig. 1.

With this class of manufacturing techniques, the formation of a high-performance, low-void-content composite is dependent on both the infusion of resin into the preform and the development of good adhesion between the resin and the fibres. The infusion stage is complicated by the fact that resin flow actually occurs at two distinct scales in the preform: the macroscopic flow of resin through the preform and the microscopic wet-out of individual fibres that make up the preform [5]. Similarly, the mechanisms of adhesion are complex and synergistic in nature, depending largely on the chemical composition of the resin and the fibre, including any sizing that may be used to enhance bonding. However, it is a well-established fact in polymer composites that wetting of the fibre surface by the resin is a prerequisite for good adhesion due to the short-range nature of intermolecular forces [6]. In this study, we investigate aspects of both permeability and fibre wetting as related to the fabrics and preforms used in RTM.

2. Background

Mould filling in LM [7, 8] is typically described by the two-dimensional form of Darcy's Law

$$\begin{pmatrix} \bar{u} \\ \bar{v} \end{pmatrix} = -\frac{1}{\eta_{\text{eff}}} \begin{pmatrix} K_{xx} & K_{xy} \\ K_{yx} & K_{yy} \end{pmatrix} \begin{pmatrix} \dfrac{\partial P}{\partial x} \\ \dfrac{\partial P}{\partial y} \end{pmatrix} \quad (1)$$

where $\bar{u}$ and $\bar{v}$ are the gap-wise averaged velocities, η_{eff} is the effective viscosity of the fluid, K_{ij} is the permeability tensor, and P is the pressure. Thus, the progression of the flow front depends on a number of factors such as the fluid characteristics (viscosity and reaction kinetics) and the processing conditions (mould temperature and injection pressure or flow rate), but it is also a function of the part geometry (size and shape) and the mould design (inlet and vent locations). While these issues dictate how the resin is introduced into the mould cavity, the rheological behavior of the resin, and the rate of resin infusion into

0022–2461 © *1995 Chapman & Hall*

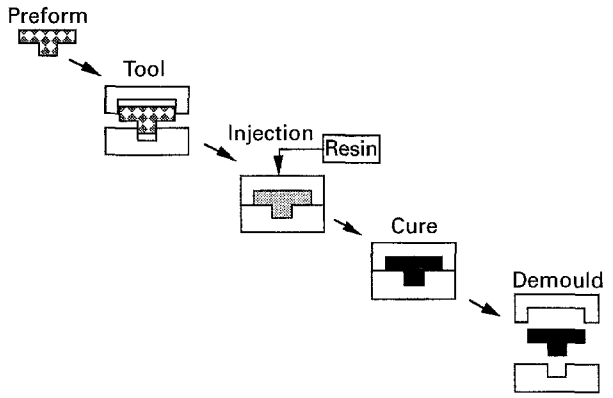

Figure 1 Schematic of liquid moulding process.

the preform, the flow of resin from the injection point is primarily dependent on the permeability of the preform. Here, permeability may be defined as a measure of the ease with which the resin flows through the reinforcement, and hence it reflects the influence of the preform's microstructure on the processing of RTM parts.

In composites processing, a variety of theoretical models, both analytical [9–11] and numerical [12–14], have been proposed to predict permeability as a function of structure. While these models work well for predicting the resistance to flow through idealized particle and fibre (i.e. perfectly aligned cylinders) beds, there are considerable discrepancies between the model predictions and experimental data for flow through real fibre beds (i.e. fabrics typically used in RTM). These discrepancies are due to the non-uniformities associated with fibre packing, bundle size, fibre alignment, and fibre volume fraction [15, 16]. Until more accurate models are developed that take into account the stochastic nature of these materials, fabric permeabilities must be determined experimentally.

3. Previous work

Previous experimental studies of fabric permeability have used idealized, Newtonian fluids such as corn syrup [17], silicone oil [18], corn oil [19], tap water [20], and DOP (diphenyloctylphthalate) oil [21]. Adams *et al.* [22] were perhaps the first investigators to use an actual resin system (Epon ™828 epoxy) when they measured the in-plane permeabilities of woven fabrics with PET (polyethyleneterephthalate), polypropylene, and nylon fibres. However, these reinforcing fibres are seldom, if ever, used in LM. For the fibres and resin systems used in LM, mere physical infusion of the preform by the injected resin does not ensure that sufficient wetting has been achieved. The resin must not only fill the gaps between the yarn bundles but also penetrate into the fibres that constitute the yarn bundles. The thermodynamics of wetting is largely dependent on the effect of the sizing/binder used on the reinforcement as well as on the interaction between fibre and matrix systems during microscopic flow. It follows from thermodynamic criteria that the surface – and hence the interphase region formed – will seek the minimization of energy, causing the constituent systems with the lowest surface tension to concentrate in the interphasial region. Since sizings/binders are usually soluble in the resin, the chemical composition of the resin may also change during infusion, in addition to gel-induced changes. Thus, it is important that an investigation of permeability be done using the actual fibre and resin systems used in LM in order to more closely approximate the actual LM processing conditions.

4. Experimental technique

To obtain the principal in-plane permeabilities of various fabrics, radial flow experiments were conducted by injecting the test fluid into a flat plaque mould and measuring the pressure at the inlet and in both principal directions of the fabric. The mould used consisted of two 25.4-mm thick acrylic face sheets separated by a 3.175-mm aluminum spacer plate with 254 × 254-mm cavity dimensions. Pressures opposite the inlet and in each of the principal directions were measured by transducers mounted in the bottom acrylic plate. A predetermined number of fabric layers, with a pre-cut hole in the centre that was aligned with the inlet, were placed within the spacer plates and between the acrylic face sheets. The pre-cut hole was employed to ensure an even pressure distribution and minimize the influence of the through-thickness permeability, K_{33}, on the measurement of in-plane permeabilities. The entire setup was bolted together and inspected to ensure that the desired preform compaction was achieved. A hydraulic pump connected to a piston/cylinder apparatus (constant flow rate injection) was employed to meter the fluid into the mould cavity at a rate of 16.2 $cm^3 s^{-1}$. This flow rate is typical of industrial rates used to fill tools but is still within the range of creeping flows where Darcy's Law is valid. Pressures were sampled five times per second through the use of a Macintosh SE30 computer with an Analog Connection Quick Log data acquisition program. The test was stopped once the fluid touched a mould wall to ensure against the effects of channelling and pressure buildup. In addition, flow visualization allowed the principal directions of the fabrics to be identified. This is extremely valuable, as the principal in-plane permeability directions do not necessarily coincide with the fibre directions, as recently noted by Parnas [23]. The entire experimental setup is shown in Fig. 2.

In the initial portion of this study, an actual LM resin (Derakane ™411-C50 vinyl ester) was used as the permeant. This fluid was characterized with a digital viscometer at room temperature over a range of shear rates from 1 to 20 s^{-1}. The resin displayed Newtonian behaviour over this range of shear rates, and its viscosity was determined to be 135 mPa s.

A variety of E-glass fabrics representative of those commonly used in LM were selected for testing: continuous strand mat, biaxial (0°/90°) knitted fabric, biaxial knitted fabric plus a layer of chopped strand mat (0°/90°/C), bias biaxial (± 45°) knitted fabric, and unidirectional woven fabric. The structural characteristics of these fabrics are provided in Table I [24, 25].

Each of the fabrics tested in this study could be compressed to various extents to alter the porosity. For instance, in these experiments the porosity of the continuous strand mat ranged from 71.8% (28.2% fibre volume fraction or five layers of fabric within the 3.175-mm thick mould cavity) to 83.1% (16.9% fibre volume fraction or three layers of fabric within the same mould cavity). The ranges chosen for each fabric are a function of the minimum fibre volume fraction that can be used while avoiding gross fibre movement (i.e. rearrangement of the fibres within the preform caused by the pressure of the infusing resin) and resin channelling (fluid flow between the layers of the preform due to insufficient compaction), and the maximum fibre compaction that can be achieved prior to deflection of the acrylic mould.

5. Data reduction

Permeabilities were determined using the data reduction scheme proposed by Bruschke [26], wherein the continuity equation for incompressible flow

$$\frac{\partial u}{\partial x} + \frac{\partial v}{\partial y} = 0 \tag{2}$$

is combined with the superficial velocities in the principal directions

$$u = \frac{K_{11}}{\eta}\frac{\partial P}{\partial x} \tag{3a}$$

and

$$v = \frac{K_{22}}{\eta}\frac{\partial P}{\partial y} \tag{3b}$$

to obtain

$$K_{11}\frac{\partial}{\partial x}\left(\frac{1}{\eta}\frac{\partial P}{\partial x}\right) + K_{22}\frac{\partial}{\partial y}\left(\frac{1}{\eta}\frac{\partial P}{\partial y}\right) = 0 \tag{4}$$

This equation was mapped into a circular domain by a simple co-ordinate transformation and then solved for the pressure as a function of the flow front location and time. By transforming this equation back to the original domain, an expression (Equation 5)

$$P(x, y) = \frac{Q}{4\pi h}\frac{1}{(K_{11}K_{22})^{1/2}}\eta \ln\frac{Q}{\pi h} \times \frac{1}{(K_{11}K_{22})^{1/2}}t + \left(\frac{x_0^2}{K_{11}} + \frac{y_0^2}{K_{22}}\right) \times \left(\frac{x^2}{K_{11}} + \frac{y^2}{K_{22}}\right)^{-1} \tag{5}$$

for the pressure, P, at any point (x, y) in the mould was determined. In this expression, Q is the volumetric flow rate, h is the mould thickness, t is the time, and x_0 and y_0 are the size of the pre-cut hole. This equation is valid only for Newtonian fluids, although Bruschke [26] does derive a similar relation for power-law fluids.

To calculate permeabilities, Equation 5 is applied at the locations of the pressure transducers and fit to the

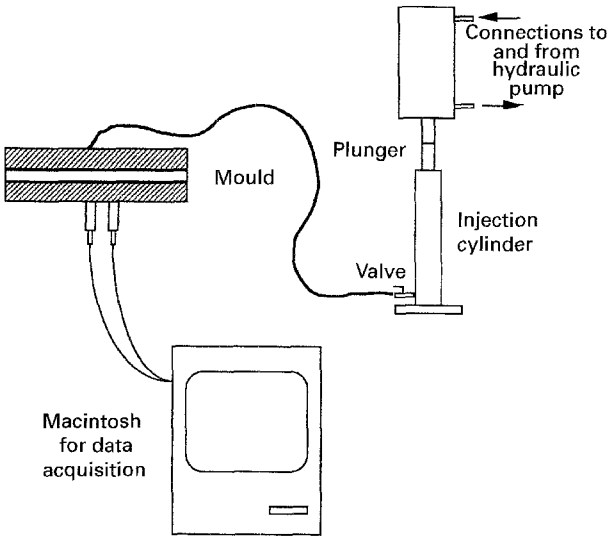

Figure 2 Schematic of the permeability apparatus.

TABLE I Structural characteristics of the fabrics tested [24, 25]

Fabric supplier and type	Fabric architecture	Warp wt %	EPI[a]	Weft wt %	EPI[a]	Stitching thread wt %	CPI[b]	Overall fabric wt. (g m^2)
Hexcel CD180	Biaxial 0°/90° knit	54	6.0	42	11.0	4	7	686
Hexcel CDM1808	Biaxial knit plus mat (0°/90°/C)	36	6.0	35	10.9	1	7	912
Hexcel DB170	Biaxial ± 45° knit	47	9.9	47	9.9	5	6	595
Hexcel A130	Unidirectional woven	96	10.0	4	1.0	Not applicable		438
Certain Teed U816	Continuous strand mat	Not applicable		Not applicable		Not applicable		450

[a] EPI = ends per inch.
[b] CPI = courses per inch.

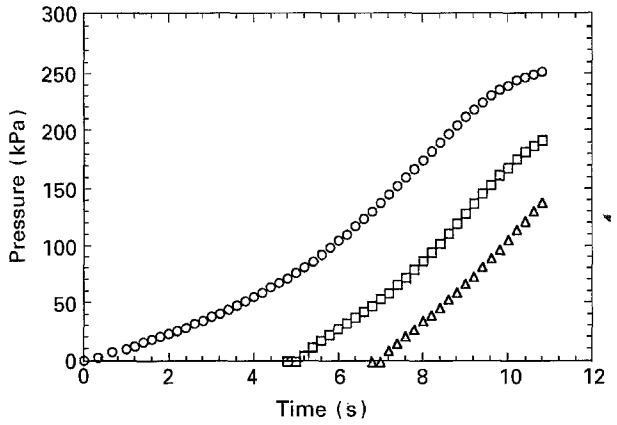

Figure 3 A typical set of pressure versus time curves from the radial flow permeability experiments. ○ inlet transducer; □ X transducer: △ Y transducer.

experimental pressure versus time curves using the permeabilities as fitting parameters. A typical pressure versus time curve is shown in Fig. 3. Finally, an iterative nonlinear curve fitting technique is used to obtain the best fit.

6. Fabric permeabilities measured with a vinyl ester resin

The principal in-plane permeabilities of the continuous strand mat are given in Table II and shown in Fig. 4 as a function of porosity. Although this material is generally considered to be isotropic in the plane of the fabric, the 2-direction permeability was consistently higher, on the order of 10%, than the 1-direction permeability. Thus, the continuous strand mat does exhibit some anisotropy; however, with the standard deviations given in Table II, no firm conclusions can be drawn with regard to this aspect. The scatter in this data may be attributed to local variations in the fibre architecture such as the fibre orientation, the fibre diameter, the number of fibres within a yarn bundle, etc.

Fig. 5 demonstrates the influence of fabric compressibility on the in-plane permeabilities of the biaxial (0°/90°) knitted fabric. As expected, this fabric exhibits a great deal of anisotropy (i.e. K_{11} was much greater than K_{22}) over the range of porosities tested (Table III). This is a manifestation of the structural characteristics of this fabric, as 54% of the fabric weight comes from the 0° fibres, while only 42% of the fabric weight comes from the 90° fibres. As shown in Table I, the remainder, 4%, of the weight of the fabric represents the polyester stitching thread that holds the 0° and the 90° yarn bundles together.

The in-plane permeabilities of the biaxial bias ($\pm 45°$) knitted fabric determined with the vinyl ester resin are shown in Fig. 6. With this fabric, there was considerable scatter in the data (Table IV), especially at a porosity of 63.4%. This seems to be a manifestation of the tendency of the biaxial bias knitted fabric to shear or alter its fibre orientation when load is applied in either of the principal directions such as during the loading of the preform into the mould cavity. Even with this scatter, a trend can be identified with regard

TABLE II Permeability data for the continuous strand mat determined with the vinyl ester resin

Porosity (%)	$K_{11}(\times 10^{-9})(m^2)$	$K_{22}(\times 10^{-9})(m^2)$
71.8	4.63 ± 0.71	5.20 ± 0.98
77.4	5.74 ± 0.62	6.37 ± 0.22
83.1	7.35 ± 0.21	8.32 ± 0.57

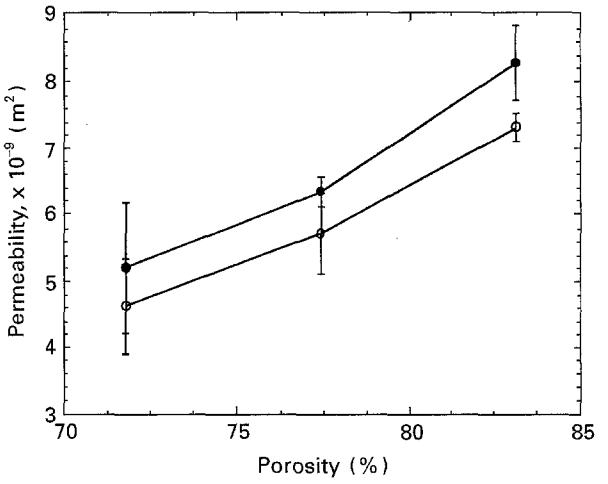

Figure 4 In-plane permeabilities of continuous strand mat determined with the vinyl ester resin. ○ K_{11}; ● K_{22}.

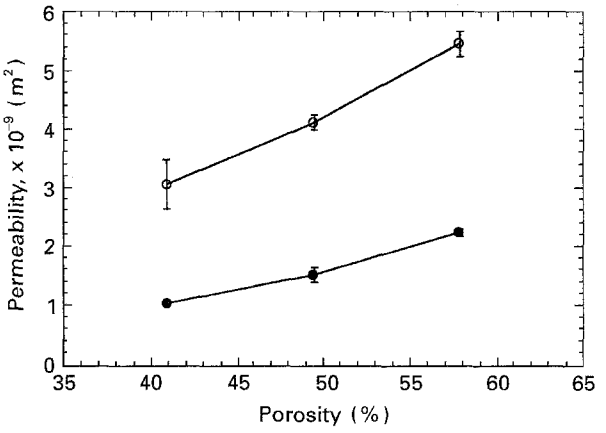

Figure 5 In-plane permeabilities of the biaxial (0°/90°) knitted fabric determined with the vinyl ester resin. ○ K_{11}; ● K_{22}.

TABLE III Permeability data for the biaxial (0°/90°) knitted fabric determined with the vinyl ester resin

Porosity (%)	$K_{11}(\times 10^{-9})(m^2)$	$K_{22}(\times 10^{-9})(m^2)$
42.7	3.08 ± 0.43	1.04 ± 0.05
49.4	4.15 ± 0.12	1.54 ± 0.12
57.8	5.50 ± 0.21	2.26 ± 0.06

to the permeability of this fabric as a function of porosity. The 1-direction permeability was consistently higher than the 2-direction permeability. This may be attributed to the chain stitches that hold the $+45°$ and $-45°$ fibres together and run down the length of the fabric in the 1-direction. In addition, increasing the porosity (or equivalently, decreasing the fibre volume fraction) led to an almost linear increase in both K_{11} and K_{22}.

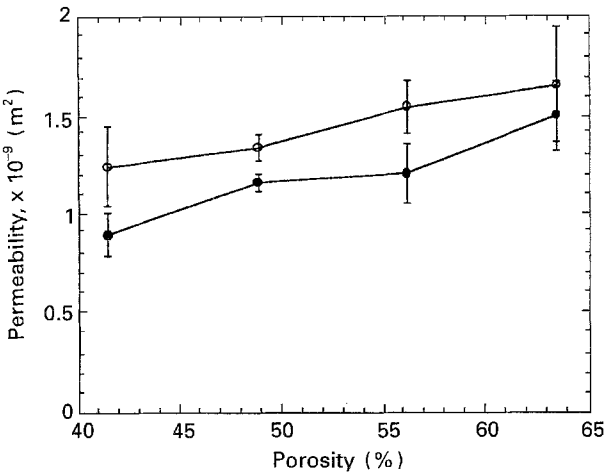

Figure 6 In-plane permeabilities of the bias biaxial (± 45°) knitted fabric determined with the vinyl ester resin. ○ K_{11}; ● K_{22}.

TABLE IV Permeability data for the bias biaxial (± 45°) knitted fabric determined with the vinyl ester resin

Porosity (%)	$K_{11}(\times 10^{-9})(m^2)$	$K_{22}(\times 10^{-9})(m^2)$
41.4	1.25 ± 0.20	0.90 ± 0.11
48.8	1.35 ± 0.07	1.17 ± 0.04
56.1	1.56 ± 0.14	1.22 ± 0.15
63.4	1.68 ± 0.29	1.52 ± 0.18

TABLE V Permeability data for the biaxial (0°/90°/C) knitted fabric plus a layer of chopped strand mat determined with the vinyl ester resin

Porosity (%)	$K_{11}(\times 10^{-9})(m^2)$	$K_{22}(\times 10^{-9})(m^2)$
45.3	1.52 ± 0.24	0.59 ± 0.12
53.1	2.57 ± 0.19	0.77 ± 0.12

The overall permeability data determined with the vinyl ester resin for the five fabrics as a function of porosity is provided in Tables II–VI. This data is also shown graphically in Fig. 7. Even though the fibres are oriented randomly in the continuous strand mat, its principal in-plane permeabilities are much greater than any of the other fabrics tested. This material's low resistance to flow may be explained by the porous nature (i.e. the low fibre volume fraction) relative to the more dense directional fabrics. While the directional fabrics appear to be lumped together in terms of their permeability–porosity relationships, this is not entirely true. Although the 2-direction permeability of the biaxial (0°/90°) knit is similar to the bias biaxial (± 45°) knit, their 1-direction permeabilities differ by a minimum of 146%. Thus, a designer cannot simply substitute one material for another in order to meet performance requirements, unless due consideration is given to the effect of this substitution on the processing of the part. Fig. 7 is extremely valuable during preform design, as it is basically a structure-processing map that simultaneously allows the materials (and structural) designer to make trade-offs between the closely coupled structural and infusion criteria. Here, the influence of the fibre architecture (or the structure) on processing may be evaluated based on how the permeability changes with the material, fibre orientation, fibre volume fraction, etc.

TABLE VI Permeability data for the unidirectional woven fabric determined with the vinyl ester resin

Porosity (%)	$K_{11}(\times 10^{-9})(m^2)$	$K_{22}(\times 10^{-9})(m^2)$
56.8	4.83 ± 0.31	0.61 ± 0.02
62.1	5.39 ± 1.03	1.05 ± 0.12

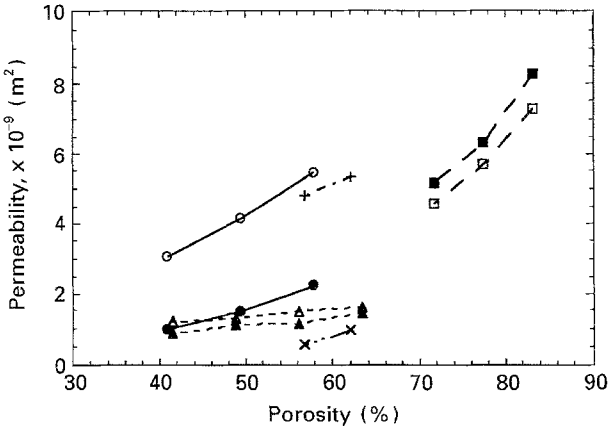

Figure 7 In-plane permeabilities of a variety of fabrics that are typically used in liquid moulding. The permeabilities were determined with a vinyl ester resin as the test fluid. ○ K_{11} (0/90); ● K_{22} (0/90); □ K_{11} (CoSM); ■ K_{22} (CoSM); △ K_{11} (± 45); ▲ K_{22} (± 45); + K_{11} (Uni); × K_{22} (Uni).

7. Effect of test fluid on permeability

In the previous section, the permeabilities of a variety of reinforcing fabrics were characterized with an actual LM resin system (Derakane™ 411-C50 vinyl ester). However, most investigations of fabric permeability have employed idealized test permeants rather than actual resin systems [17–22]. In order to better understand the role of the test fluid in permeability measurement, the permeability experiments were repeated with two idealized test fluids (SAE 10W-30 motor oil and diluted corn syrup) for both the continuous strand mat and the bias biaxial (± 45°) knitted fabric. As with the vinyl ester resin, the idealized test fluids were characterized with the digital viscometer at room temperature over a range of shear rates from 1 to 20 s^{-1}. Both the motor oil and the diluted corn syrup displayed Newtonian behaviour over this range of shear rates, with viscosities of 155 and 190 MPa s, respectively. (The corn syrup was diluted with deionized water to arrive at this viscosity). Using the experimental procedure and the data reduction method outlined in the previous sections, the permeabilities of the continuous strand mat and the bias biaxial (± 45°) knitted fabric were each determined at two porosity levels.

The principal in-plane permeabilities of the continuous strand mat and the bias biaxial (± 45°) knitted fabric are shown in Figs 8 and 9, respectively, as a function of the test fluid (vinyl ester, motor oil, and diluted corn syrup). For both fabric types, the

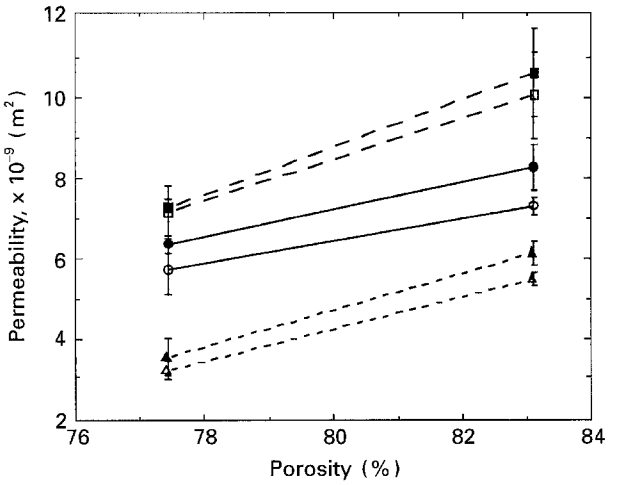

Figure 8 Comparison of the in-plane permeabilities of the continuous strand mat as a function of porosity and test fluid. [Vinyl ester (VE), motor oil (MO) and corn syrup (CS)]. ○ K_{11} (VE); ● K_{22} (VE); □ K_{11} (MO); ■ K_{22} (MO); △ K_{11} (CS); ▲ K_{22} (CS).

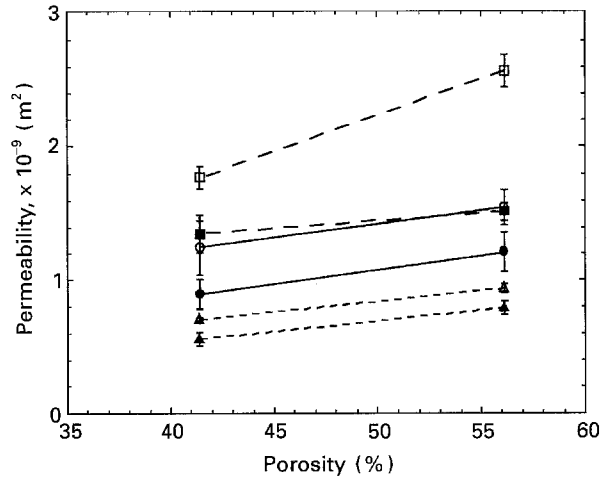

Figure 9 Comparison of the in-plane permeabilities of the bias biaxial (± 45°) knitted fabric as a function of porosity and test fluid. [Vinyl ester (VE), motor oil (MO) and corn syrup (CS)]. See Fig. 8 for key.

permeabilities show a strong dependence on the test fluid. The highest values of permeability, in both directions, correspond to the use of motor oil and the lowest to the use of corn syrup. The significant scatter in permeability data for the ± 45° fabric may be related to the tendency of the bias knitted fabric to easily shear under an applied load. It should be mentioned that although the viscosity of the test fluids is used in the determination of permeability (Equation 5), the experimental trends in permeability do not correspond with the trend in viscosity data, which showed an increase from vinyl ester (135 MPa s) to motor oil (155 MPa s) to corn syrup (190 MPa s). Based on a visual inspection of the fabrics after each permeability experiment, the variation in the principal in-plane permeabilities with test fluid seems to be related to fibre wetting (i.e. the affinity of the test fluid for the fibre).

8. The role of fibre wetting in permeability measurements

The wet-out of a reinforcement is a measure of how well the resin system impregnates the reinforcement. This is of special importance in composites because good wet-out is a necessary (although not sufficient) condition for the formation of a good bond between the matrix and reinforcement phases, and hence the structural integrity and performance of the composite. In RTM, this assumes special importance because the fibres must have appropriate compatibility for the resin system (achieved through the use of sizings) in order to enable wet-out as the flow front progresses through the perform. The wetting of a fibre surface by a fluid may be described by the three-phase thermodynamic equilibrium between the solid, liquid, and vapour phases (Fig. 10), and the requisite interfacial forces can be related by the Young–Dupré [6, 27] equation

$$\gamma_{sv} = \gamma_{sl} + \gamma_{lv}\cos\theta \qquad (6)$$

Here, γ_{sv}, γ_{sl} and γ_{lv} are the surface free energies (also known as the surface tensions) between the solid and the vapour, the solid and the liquid, and the liquid and the vapour, respectively. In addition, θ is the equilibrium contact angle the liquid forms with the solid, and it provides some information about the attraction of the liquid for the solid. When $\theta > 0°$, the liquid may be termed non-spreading, and it will not spontaneously wet the solid. It should be emphasized that under this condition, it is still possible for the liquid wetting to occur; however, pressure must be applied to the liquid in order to spread it over the solid surface [27]. There is always some wetting when a liquid comes into contact with a solid, except for the case $-1 \leqslant \cos\theta < 0$, where the attraction of the solid for the liquid is less than the liquid for itself [28]. On the other hand, when $\theta = 0°$ the liquid is said to spread over the solid surface, and the Young–Dupré equation (Equation 6) cannot be used to predict the relationship between the surface free energies.

Despite the attractiveness of using contact angle as a direct indication of the degree of wetting, it is emphasized that wetting is actually the consequence of three independent parameters (γ_{sv}, γ_{sl} and γ_{lv}), and thus the contact angle interpretation is complicated by the interaction terms. The most direct measure of wetting is the work of spreading, W_s, which is also known as the spreading coefficient [29] and may be given as

$$W_s = W_{sl} - W_{ll} \qquad (7)$$

where W_{ll} is the work of cohesion of the fluid and W_{sl} is the work of adhesion. Substitution of the surface free energies results in

$$W_s = \gamma_{sv} - \gamma_{sl} - \gamma_{lv} \qquad (8)$$

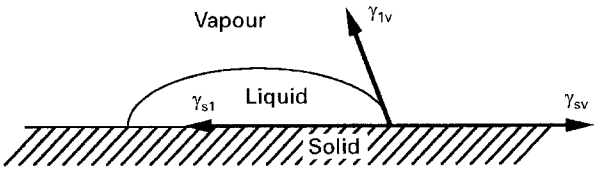

Figure 10 The three-phase thermodynamic equilibrium condition that exists for a drop of liquid resting at equilibrium on a solid surface (After Kinloch [27]).

Fowkes [30] proposed that the surface free energy of a pure phase was composed of a variety of interactions, including dispersive (or London) forces, polar (or Keesom) forces, acid–base interactions, hydrogen bonding, dipole–dipole interactions, and induced dipole–dipole interactions. Both dispersive (superscript D) and non-dispersive (or polar, superscript P) forces between the solid and the liquid can be accounted for through the use of a geometric mean to determine the solid–liquid surface free energy [30–32] as

$$\gamma_{sl} = \gamma_{sv} + \gamma_{lv} - 2(\gamma_{sv}^{D}\gamma_{lv}^{D})^{1/2} - 2(\gamma_{sv}^{P}\gamma_{lv}^{P})^{1/2} \quad (9)$$

The assumptions used in this approach are not without criticism. Most notably there has been some objection to the use of the geometric mean to predict polar interactions. This approach assumes that all non-dispersive interactions are polar and ignores additional interfacial interactions that may be important in some systems. However, despite the sound criticism, the approach outlined above does give insight into the thermodynamic aspects of surface interactions and wetting.

9. Characterization of surface interactions

A dynamic contact angle analyser, based on the micro-Wilhemy technique [28], was used to determine the polar and dispersive components as well as the total surface free energies of the fibres and test fluids under consideration. For the determination of surface tensions of the three test fluids (vinyl ester, motor oil, and diluted corn syrup), glass slides and Teflon® (PTFE) samples were used as the solid test surfaces. The solid samples were immersed at a rate of 75 $\mu m\,min^{-1}$ into the test fluids (the experiments were repeated eight times for each solid/liquid combination). Since the fluids spread over the high energy surface of the glass slides (i.e. zero contact angle), the balance of forces

$$F = \frac{\gamma_{lv} P \cos\theta}{g} \quad (10)$$

was used to determine the surface tension γ_{lv}, of each of the fluids. Here, F is the force, P the perimeter of the solid and g the gravitational acceleration. Teflon, a highly dispersive solid (181.0 $\mu N\,cm^{-1}$ dispersive and 9.3 $\mu N\,cm^{-1}$ polar), was used to determine the dispersive component of the fluid surface free energy.

Following Kaeble [32], the Young–Dupré equation (Equation 6) was combined with equation (15) such that

$$1 + \cos\theta = \frac{2(\gamma_{sv}^{D}\gamma_{lv}^{D})^{1/2}}{\gamma_{lv}} + \frac{2(\gamma_{sv}^{P}\gamma_{lv}^{P})^{1/2}}{\gamma_{lv}} \quad (11)$$

Since the total surface tension of the fluids, the surface free energy of the dispersive solid, and the contact angles of the test fluids with the dispersive solid are known, simultaneous equations based on Equation 11 can be solved for the polar and dispersive components of each liquid's surface free energy. The values in Table VII were determined based on the receding data, since this curve yields "the most wettable value and more closely approximates a zero contact angle" [33].

TABLE VII Polar, dispersive and total surface free energies of the test fluids used in the permeability experiments

Test fluid	γ_{lv}^{P} ($\mu N\,cm^{-1}$)	γ_{lv}^{D} ($\mu N\,cm^{-1}$)	γ_{lv} ($\mu N\,cm^{-1}$)
Diluted corn syrup	426 ± 40	231 ± 40	657 ± 24
Motor oil	29 ± 20	293 ± 20	322 ± 12
Vinyl ester	12 ± 10	342 ± 10	354 ± 70

TABLE VIII Polar, dispersive and total surface free energies of the fibres that comprise the continuous strand mat based on contact angle measurements with deionized water, glycerol and formamide

Single fibres from fabric type	γ_{sv}^{P} ($\mu N\,cm^{-1}$)	γ_{sv}^{D} ($\mu N\,cm^{-1}$)	γ_{sv} ($\mu N\,cm^{-1}$)
Continuous strand mat	288 ± 15	195 ± 26	483 ± 41

Table VII indicates that the total surface free energy increased as the test fluid changed from motor oil to vinyl ester to diluted corn syrup. In addition, both the motor oil and the vinyl ester resin were highly dispersive fluids, while the diluted corn syrup was a highly polar fluid. Since the corn syrup was diluted with deionized water, which was characterized as 225.0 $\mu N\,cm^{-1}$ dispersive and 503 $\mu N\,cm^{-1}$ polar for a total surface free energy of 728.0 $\mu N\,cm^{-1}$ the polar nature of this test fluid was expected.

10. Surface free energies of fibres

Micro-Wilhemy measurements were performed on single fibres, which were extracted from the continuous strand mat, with several probe liquids of known polar and dispersive components. Deionized water, glycerol, and formamide were selected as probe liquids because the surface free energies of these fluids were large enough that the fluid would not spread over the fibre surface (i.e. the contact angle was greater than zero). Single fibres were immersed into these liquids at a rate of 10 $\mu m\,min^{-1}$. The diameter of the fibres that comprise the continuous strand mat was determined by optical microscopy to be 18 ± 1 μm. The fibre diameter was used to calculate the perimeter of the solid in Equation 10.

By measuring the contact angle that each of the probe liquids forms with the glass fibres, the polar and dispersive components of the surface free energies can be determined from Equation 11 by forming a set of simultaneous equations. The advancing contact angles were employed in these calculations, as the probe liquids may spread over the surface of the fibre during the receding portion of the experiment. The total surface free energy is then simply the sum of the polar and dispersive components (Table VIII). The results are seen to be consistent with the limited data reported in the literature [34, 35].

11. Fibre–test fluid interactions

From the polar, dispersive, and total surface free energies of the test fluids (Table VII) and the fibres (Table VIII), Equations 6, 8, and 9, the work of adhesion (W_{sl}), the work of spreading (W_s) and the contact angle (θ) may be calculated for each of the fibre–test fluid interactions as shown in Table IX. In order to verify these results, the contact angles that the test fluids make with the single glass fibres were measured following the procedure described previously and the results compared with calculated values in Table X. The advancing contact angle was used for these comparisons because the physics of this portion of the wetting experiment most closely resembles the radial flow permeability test, as both experiments involve the advancement of a fluid into a dry, non-saturated medium. There is a direct correlation between the results of the surface characterization study and the permeability tests with the three test fluids. The measurements made with the motor oil yielded the highest principal in-plane permeabilities, and in the wetting experiments this fluid was shown to be attracted to the glass fibres from the continuous strand mat (i.e. the work of spreading was greater than zero). As the test fluid was changed from the motor oil to vinyl ester to diluted corn syrup, both the principal in-plane permeabilities and the work of spreading decreased (Fig. 11). For both the vinyl ester and the diluted corn syrup, the work of spreading was negative. This indicates that pressure must be applied to these fluids in order to get them to wet the fibre surfaces.

TABLE IX Calculated work of adhesion, work of spreading, and contact angles for glass fibres from the continuous strand mat and the test fluids

Test fluid	W_{sl} ($\mu N\,cm^{-1}$)	W_s ($\mu N\,cm^{-1}$)	θ (Degrees)
Diluted corn syrup	1125	− 189	44·6
Motor oil	658	16	Spreads
Vinyl ester	634	− 74	37.7

TABLE X Comparison of the measured and calculated contact angles for glass fibres from the continuous strand mat and the test fluids

Test fluid	$\theta_{calculated}$ (Degrees)	$\theta_{measured}$ (Degrees)
Diluted corn syrup	44.6	45.4 ± 6.3
Motor oil	Spreads	Spreads
Vinyl ester	37.7	31.5 ± 4.4

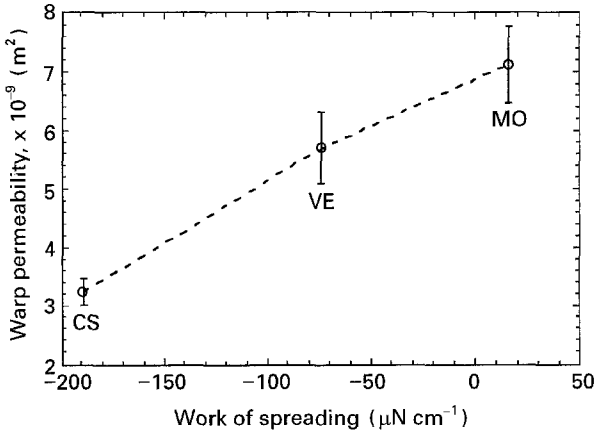

Figure 11 The relationship between permeability (macroscopic flow) and fibre wetting (microscopic flow) for continuous strand mat at a porosity of 77.4%.

12. Conclusions

Traditionally, fibre–resin wetting and adhesion have not been considered a major processing-related problem in polymer composites because the fibre and resin are intimately coupled when obtained in the preimpregnated tape form. However, in processes such as LM, fibres and resin are separate until the start of processing, and hence issues of permeability (or the macroscopic flow of resin through the preform) and fibre wet-out (or the microscopic flow of resin within a fibre bundle) and their interaction (the balance of macroscopic and microscopic aspects of flow) become much more important. Commercial glass fibres are coated with sizings and binders, which are combinations of silanes, organo-function silane coupling agents, film formers, lubricants, and anti-static agents ranging from 0.1 to 10 μm in thickness [36]. The presence of these materials on the fibre surface affects not only performance attributes but also the processing of RTM composites.

Recently, a few investigators have examined the influence of capillary pressure on the impregnation of fibrous reinforcements; however, mixed results have been obtained in these studies. Ahn *et al.* [34] determined that the capillary pressure was sensitive to variations in porosity, especially when low porosity reinforcements were employed. They observed a maximum capillary pressure of 37.0 kPa, which should be accounted for in permeability experiments. On the other hand, Skartsis *et al.* [35] suggested that during the transverse flow through aligned carbon fibre beds, no correction for capillary pressure was needed; however, a very limited number of experiments was conducted to verify their predictions. Thus, the contribution of capillary pressures to the overall driving force during the resin infusion/impregnation portion of the LM process is still unclear. The results of this investigation demonstrate that surface effects are important, and capillary effects may explain the differences in principal in-plane permeabilities measured with the vinyl ester resin, the motor oil, and the diluted corn syrup. Until a more complete understanding of test fluid–fibre interactions is developed, it appears that fabrics should be characterized with the actual LM resin selected for a given application, since permeability measurements made with other idealized fluids yield only apparent permeabilities.

References

1. M. H. NAITOVE, *Plast. Technol.* **28** (1982) 79.
2. I. SAYAMA, I. NOMURA, K. TABEI and S. GOTOH, in Proceedings of the Society of the Plastics Industry/Reinforced

Plastics-Composites Institute 36th Annual Technical Conference, Cincinnati, OH (1981) p. 1.
3. C. F. JOHNSON, N. G. CHAVKA, R. A. JERYAN, C. J. MORRIS and D. A. BABBINGTON, in Proceedings of the Third Annual ASM/ESD Advanced Composites Conference, Detroit, MI (ASM International, Metals Park, Ohio, USA, 1987) p. 197.
4. C. F. GRIFFITH, W. E. HARVILL, R. R. JOHNSON and R. E. BOHLMANN, *Aerospace America* **26** (1988) 28.
5. R. S. PARNAS and F. R. PHELAN, Jr., *SAMPE Quart.* **22** (1991) 53.
6. S. WU, "Polymer interface and adhesion" (Marcel Dekker, Inc., New York, 1982).
7. J. P. COULTER and S. I. GÜÇÉRI, *J. Reinf. Plast. Compos.* **7** (1988) 200.
8. M. V. BRUSCHKE and S. G. ADVANI, *Polym. Compos.* **11** (1990) 398.
9. P. C. CARMAN, *Trans. Inst. Chem. Eng.* **15** (1937) 150.
10. R. J. MARSHALL and A. B. METZNER, *Ind. Engng Chem. Fund.* **6** (1967) 393.
11. Z. KEMBLOWSKI and M. MICHNIEWICZ, *Rheol. Acta* **18** (1979) 730.
12. E. M. SPARROW and A. L. LOEFFLER, *AIChe* J. **5** (1959) 325.
13. A. S. SANGANI and A. ACRIVOS, *Int. J. Multiphase Flow* **8** (1982) 193.
14. R. E. LARSON and J. L. L. HIGDON, *J. Fluid Mech.* **166** (1986) 449.
15. J. G. WILLIAMS, C. E. M. MORRIS and B. C. ENNIS, *Polym. Engng Sci.* **14** (1974) 413.
16. A. S. SANGANI and C. YAO, *Phys. Fluids* **31** (1988) 2435.
17. G. Q. MARTIN and J. S. SON, in Proceedings of the Second Annual ASM/ESD Advanced Composites Conference, Detroit, MI (ASM International, Metals Park, Ohio, USA, 1986) p. 149.
18. R. GAUVIN and M. CHIBANI, *SAMPE Quart.* **21** (1990) 52.
19. Y. R. KIM, S. P. McCARTHY, J. P. FANUCCI, S. C. NOET and C. KOPPERNAES, *ibid.* **22** (1991) 16.
20. S. J. CLAUS and A. C. LOOS, in Proceedings of the American Society for Composites Fourth Annual Technical Conference, Blacksburg, Virginia (1989) p. 147.
21. L. TREVINO, K. RUPEL, W. B. YOUNG, M. L. LIOU and L. J. LEE, *Polym. Compos.* **12** (1991) 20.
22. K. L. ADAMS, B. MILLER and L. REBENFELD, *Polym. Engng Sci.* **26** (1986) 1434.
23. R. S. PARNAS, Center for Composite Materials Seminar Series, University of Delaware, Newark, DE (1992).
24. Fabric Handbook, Hexcel Corporation, Trevarno Division (1990).
25. Unifilo U816 Product Information Sheet, Vetrotex, UK (1990).
26. M. V. BRUSCHKE, PhD Dissertation, Department of Mechanical Engineering, University of Delaware, Newark, DE (1992).
27. A. J. KINLOCH, "Adhesion and adhesives: science and technology" (Chapman and Hall, London, 1987).
28. B. MILLER, in "Surface Characteristics of Fibers and Textiles, Part II", edited by M. J. Schick (Marcel Dekker, Inc., New York, 1977).
29. J. C. BERG, in "Composite Systems from Natural and Synthetic Polymers", edited by L. Salmén, A. de Ruvo, J. C. Seferis and E. B. Stark (Elsevier Science Publishers, Amsterdam, 1986).
30. F. M. FOWKES, *J. Phys. Chem.* **67** (1963) 2538.
31. F. M. FOWKES, in "Treatise on Adhesion and Adhesives", edited by R. L. Patrick (Marcel Dekker, Inc., New York, 1967).
32. D. H. KAEBLE, *J. Adhesion* **2** (1970) 66.
33. Cahn Dynamic Contact Angle (DCA) Instruction Manual, Cahn Instruments, Inc., (1992).
34. K. J. AHN, J. C. SEFERIS and J. C. BERG, *Polym. Compos.* **12** (1991) 146.
35. L. SKARTSIS, B. KHOMAMI and J. L. KARDOS, *SAMPE J.* **28** (1992) 19.
36. E. P. PLUEDDEMANN, "Silane Coupling Agents" (Plenum Press, New York, 1991).

Received 7 January
and accepted 16 September 1994